Push-pull phenoxazine-based sensitizers for p-type DSSCs: Effect of acceptor units on photovoltaic performance

Kavya Keremane, Aurélien Planchat, Yann Pellegrin, Denis Jacquemin, Fabrice Odobel, Airody Vasudeva Adhikari

Push-pull phenoxazine-based sensitizers for *p*-type DSSCs: Effect of acceptor units on photovoltaic performance

Kavya S. Keremane,[a] Aurélien Planchat,[b] Yann Pellegrin,[b] Denis Jacquemin,[b,*] Fabrice Odobel,[b,*] and Airody Vasudeva Adhikari [a,c,*]

[a] Organic Materials Laboratory, Department of Chemistry, National Institute of Technology Karnataka, Surathkal, Mangalore-575025, India

b Nantes Université, CNRS, CEISAM UMR 6230, Nantes, France

[c] Yenepoya Research Centre, Yenepoya deemed to be University, Deralakatte, Mangalore-575 018, India

*Corresponding authors e-mail: denis.jacquemin@univ-nantes.fr (Denis Jacquemin), fabrice.odobel@univ-nantes.fr (Fabrice Odobel), avachem@gmail.com (Airody Vasudeva Adhikari)

Abstract

Finding new efficient *p*-type sensitizers for NiO photocathodes is a great challenge for the development of promising low-cost tandem DSSCs. Now, the focus of researchers investigating these cells has been to create high-performance *p*-type systems. With this intention, herein, we report the design and synthesis of six new phenoxazine-based D-A configured organic dyes **PO1-6** comprising different acceptor moieties specially designed for the sensitization of mesoporous *p*-type semiconductor NiO for the construction of *p*-type dye-sensitized solar cells (*p*-DSSCs). This work includes structural, photophysical, thermal, electrochemical, theoretical, and photoelectrochemical studies of these dyes, including evaluation of their structure-property relationships. The optical studies revealed that **PO1-6** display adequate absorption and emission features in the range of 480-550 nm and 560-650 nm, respectively, with a bandgap in the order of 2.05-2.40 eV, and their thermodynamic parameters favour an efficient interfacial charge transfer involving NiO. Among the six new dyes, the device based on sensitizer **PO2** carrying electron-withdrawing 1,3-diethyl-2-thiobarbituric acid achieved the highest *PCE* of 0.031 % (J_{SC}: 0.89 mA·cm^{-2}, V_{OC}: 101 mV, and *FF*: 35 %). Conclusively, the study furnishes an understanding of the intricacies involved in the structural modification of phenoxazine-based sensitizers to further ameliorate the performance of the *p*-type DSSCs.

Keywords: DSSC; sensitizers; push-pull dyes; phenoxazine; acceptor; TD-DFT

Introduction

Over the past three decades, solar energy utilization and harvesting have played a substantial role in meeting the rising demand for the world energy crisis.[1–3] Among the new third-generation photovoltaic devices, dye-sensitized solar cells (DSSCs), comprising organic dyes, mesoporous semiconductors, and redox shuttles have witnessed substantial attention following the pioneering work of Grätzel and O'Regan in 1991.[4,5] Recently, tandem dye-sensitized solar cells, where both anode and cathode sensitized with dye molecules emerged as a promising technique for solar energy conversion with low cost and potentially higher efficiency than the conventional *n*-type DSSCs.[6–8] Nevertheless, the poor performance of *p*-type DSSCs limits the development of high-efficiency tandem solar cells, which remain hampered by several hurdles for their large-scale commercial applications.[9,10] Amongst other factors, the rapid charge recombination between holes of the photocathode NiO surface and the reduced dye or electrolyte significantly limits the power conversion efficiency (*PCE*) of *p*-type DSSCs.[11–13] Though the precise reason behind this rapid recombination is still ambiguous, it has been demonstrated in the literature that dyes can be engineered to promote the lifetime of the subsequent charge separation, thereby enhancing the current density and efficiency.[14–17] Thus, there is a growing demand for the development of new sensitizers for *p*-type DSSCs, one ultimate goal being their assembly into tandem solar cells.[18,19]

A well-known strategy to improve the performance of *p*-DSSCs is to introduce an organic dye with the "push-pull" configuration, which significantly enhances the light-harvesting and hole injection capabilities for better photoinduced intramolecular charge transfer (ICT).[20,21] The absorption and ICT characteristics of the dyes can be tuned *via* structural modification by altering their donor and acceptor units.[22–24] Among the various electron donor moieties, phenoxazine derivatives are considered to be promising candidates for *n*-type DSSC sensitization applications due to their valuable optical and electronic properties.[25,26] Indeed, the presence of electron-rich nitrogen and oxygen heteroatoms in a phenoxazine core remarkably enhances the electron-donating ability whereas its non-planar butterfly conformation significantly helps in limiting both molecular aggregation and intermolecular excimers formation.[27,28] In addition to this, the two phenyl rings typically present at a small torsion angle which allows for π-delocalization over the entire chromophore.[29] Furthermore, it has been shown that adequately substituted phenoxazine dyes can display intersystem crossing with high quantum yield leading to a triplet excited state.[30] This property is particularly relevant in the context of *p*-DSSC, which is strongly

limited by charge recombination because i) hole injection from triplet excited state could promote the formation of triplet charge-separated state possibly longer-lived than its singlet counterpart and; ii) the long lifetime of the sensitizer in triplet excited state could leverage long distance hole injection in NiO and thus simultaneously delay charge recombination.[31–34] Further, the nitrogen atom in the system can be easily substituted with a bulky long branched alkyl chain, which not only supresses the electron-hole recombination, but also diminishes the aggregation as well as solubility problems, eventually leading to improved open-circuit voltage (V_{OC}).[35,36] These features make phenoxazine a promising building block to develop sensitizers for *p*-DSSC application. To the best of our knowledge, there are no literatures reports available on phenoxazine-based organic chromophores to explore their potential as *p*-type sensitizers in NiO-based *p*-DSSCs.

In the above-described framework, we have designed six new D-A configured phenoxazine-based organic chromophores **PO1-6**, with various acceptor units, *viz*, *N*,*N*-dimethyl barbituric acid, *N*,*N*-diethyl thiobarbituric acid, malononitrile, 3-ethylrhodanine, (3,5,5-trimethylcyclohex-2-enylidene)malononitrile, and *2*-oxindole, respectively for *p*-type DSSC applications (Figure 1). The molecular engineering of these molecules involves the inclusion of electron-withdrawing group at C(3) position of the phenoxazine core as an electron acceptor unit, the carboxylic acid group at the C(7) position as an anchoring unit on the opposite side, combined with a branched alkyl chain at the N(10) atom of the phenoxazine core as a blocking agent against the electrolyte. In addition to the introduction of new phenoxazine-based dyes as a *p*-type sensitizer, this is the first report which highlights the effect of various acceptor units on recombination kinetics and photovoltaic performance of *p*-type DSSCs.

Further, the newly designed molecules were synthesized from simple starting material 10*H*-phenoxazine following a multistep synthesis pathway (Scheme 1). The schematic representation of molecular design strategy and chemical structures of new *p*-type dyes **PO1-6** along with the benchmark reference dye **P1** are shown in Figure 1. All the target dyes and their corresponding intermediates were fully characterized by ^{1}H NMR, ^{13}C NMR, FT-IR, mass spectrometry, and elemental analyses. Their photophysical, as well as electrochemical properties, were comprehensively examined by means of UV-Visible absorption, photoluminescence (PL), and cyclic voltammetric (CV) studies. Also, their thermal behavior was evaluated by TGA and DSC studies. Furthermore, the molecular geometries, molecular orbitals, charge-transfer properties, and optical spectra of **PO1-6** were theoretically investigated using density functional theory (DFT) and time-dependent density functional

theory (TD-DFT). Finally, the synthesized dyes were employed as sensitizers towards the fabrication of new NiO-based *p*-type DSSCs, and their photovoltaic performance data were assessed. Also, their quantum efficiency measurements were carried out to obtain their incident photon to current conversion efficiency (*IPCE*) spectra.

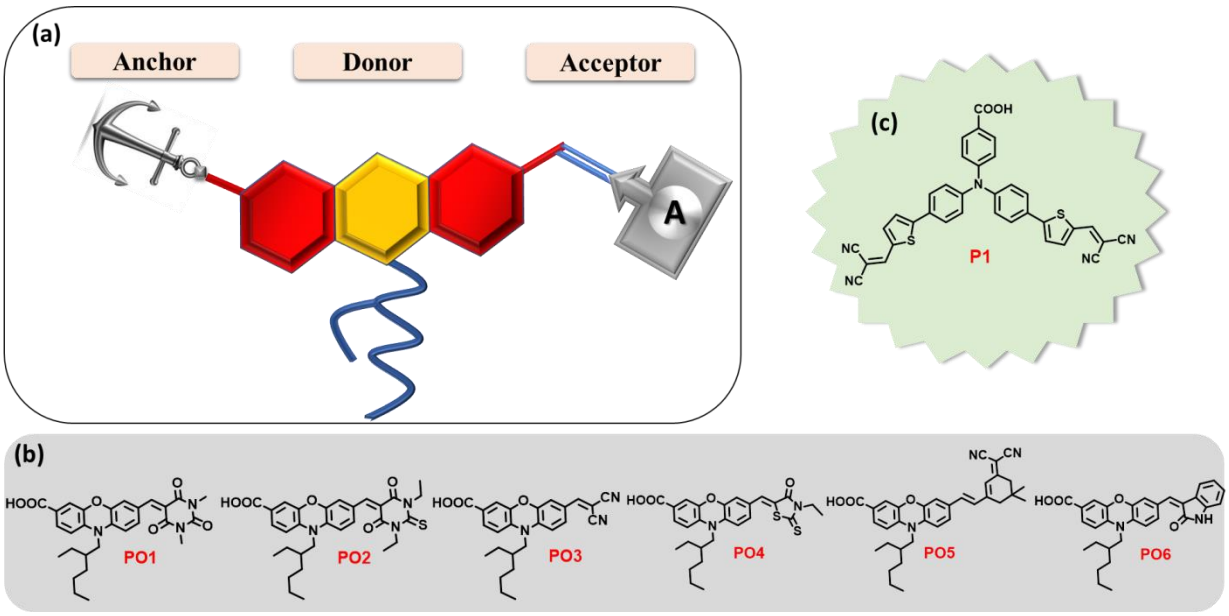

Figure 1. (**a**) Schematic representation of molecular design strategy of D-A configured new dyes **PO$_{1-6}$**, chemical structures of (**b**) new dyes **PO$_{1-6}$**, and (**c**) the benchmark reference dye **P1**

Results and discussion

Synthesis and characterization

The synthetic pathways of new phenoxazine-based organic sensitizers (**PO$_{1-6}$**) with a D-A configuration, carrying six different electron acceptor units in their structures are depicted in Scheme 1. The requested intermediate 10-(2-ethylhexyl)-10*H*-phenoxazine (**1**) was obtained from starting material 10*H*-phenoxazine by nucleophilic substitution with 2-ethylhexyl bromide in the presence of sodium hydride. This was converted to the key precursor intermediate 10-(2-ethylhexyl)-10*H*-phenoxazine-3,7-dicarbaldehyde (**2)** through the Vilsmeier-Haack reaction protocol. The intermediate **2** was oxidized to get 10-(2-ethylhexyl)-10*H*-phenoxazine-3-carboxylic acid (**3)** with the help of Ag_2O as an oxidizing agent. Then, the carboxylic group of the compound **3** was protected by esterification (Fisher ester synthesis) to give the intermediate **4**. Further, the ester **4** was formylated using the Vilsmeier-Hack reaction protocol and the crude formylated product was hydrolyzed with lithium hydroxide to get the intermediate **6**. In the final step, the target molecules **PO$_{1-6}$** were

obtained in good yield by following the Knoevenagel condensation of 10-(2-ethylhexyl)-7-formyl-10*H*-phenoxazine-3-carboxylic acid (**6**) with an active methylene compound, *viz*. *N*,*N*-dimethyl barbituric acid, *N*,*N*-diethyl thiobarbituric acid, malononitrile, 3-ethylrhodanine, (3,5,5-trimethylcyclohex-2-enylidene)malononitrile, and *2*-oxindole, respectively. The detailed synthetic procedure of all the intermediates, as well as target molecules, was given in SI. All the synthesized compounds were purified using recrystallization or column chromatography techniques. The molecular structures of the newly synthesized dyes and their intermediates were confirmed by using various spectroscopy methods (**S1-S35**, SI) and elemental analysis.

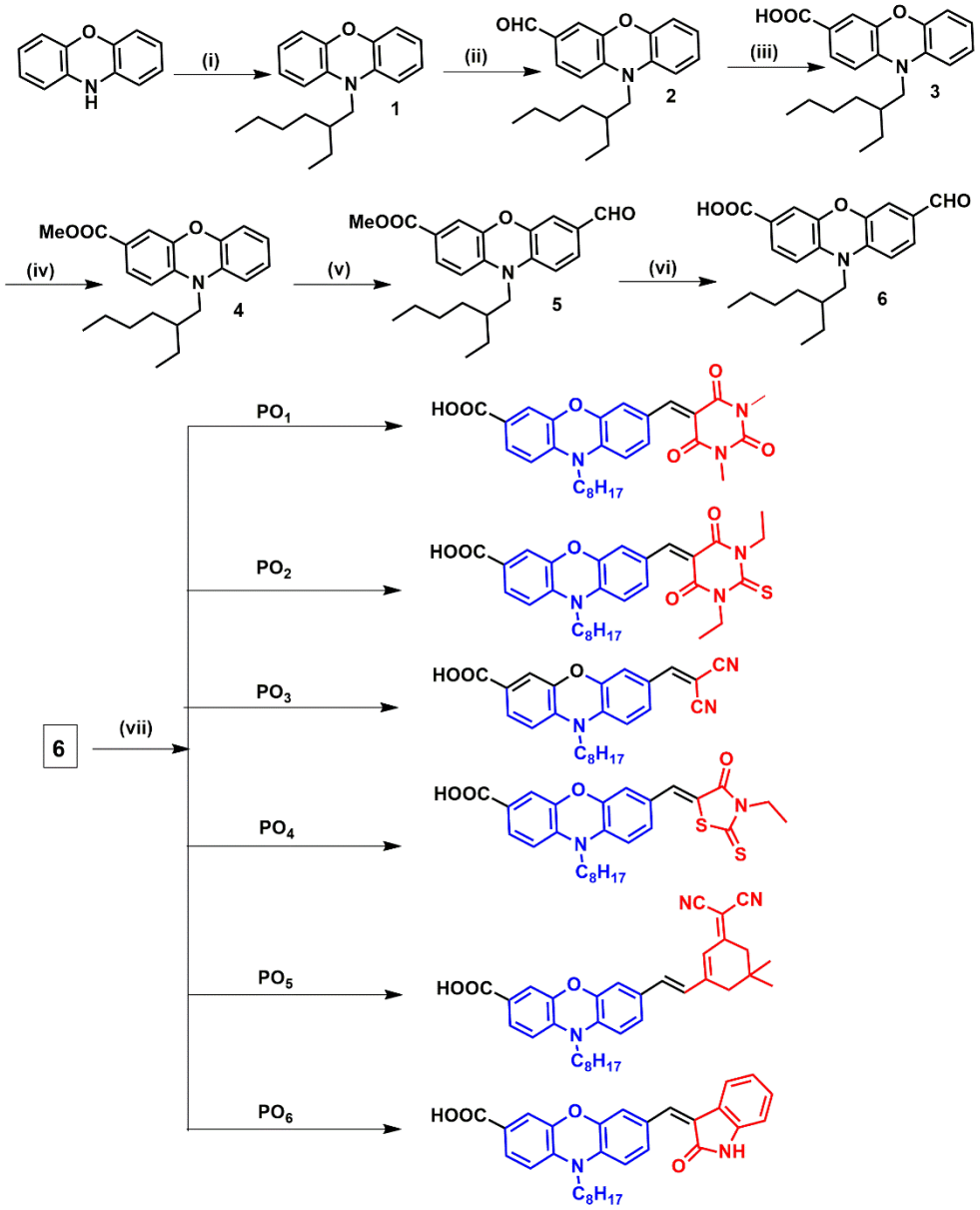

Scheme 1. Synthetic routes for the dyes **PO**$_{1\text{-}6}$: (i) 2-Ethylhexyl bromide, NaH, DMF, RT, 12 h, 97 %; (ii) $POCl_3$, DMF, RT, 12 h, 79 %; (iii) Ag_2O, NaOH, EtOH, RT, 12 h, 77 %;

(iv) MeOH, H_2SO_4, reflux, 90 %; (v) DMF, $POCl_3$, 90 ºC, 12h, 93 %; (vi) $LiOH.H_2O$, 80 ºC, 12 h, 62 %; (vii) **PO$_{1-2}$**: *N*,*N*-dimethyl barbituric acid/*N*,*N*-diethyl thiobarbituric acid, methanol, 65 ºC, 12 h, 87 %; **PO$_3$**: malononitrile, DMF, 90 ºC, 12 h, 78 %; **PO$_4$**: *N*-ethyl rhodanine, glacial acetic acid, 110 ºC, 12 h, 84 %; **PO$_5$**: (3,5,5-trimethylcyclohex-2-enylidene) malononitrile, piperidine, acetonitrile, 80-85 ºC, 12 h, 81 %; **PO$_6$**: 2-oxindole, piperidine, ethanol, 80 ºC, 12 h, 76 %.

Electronic properties

The UV-Vis absorption spectra of the new *p*-type organic chromophores **PO$_{1-6}$** obtained in 10^{-5} M $CHCl_3$ solutions are depicted in Figure 2a and key photophysical data are summarized in Table 1. The absorption spectra of dyes **PO$_{1-6}$** display two distinctive absorption bands. The absorption band in the region of 330-430 nm can be assigned to π-π^* electronic excitations localized within the phenoxazine donor, whereas the peak corresponding to the longer wavelength, *i.e.* 480-520 nm can be attributed to the intramolecular charge transfer (ICT) from the donor to the electron acceptor unit, which was further confirmed by TD-DFT calculations (*vide infra*). For the ICT band, the λ_{max} values are observed at 515 nm (**PO$_1$**), 521 nm (**PO$_2$**), 496 nm (**PO$_3$**), 510 nm (**PO$_4$**), 518 nm (**PO$_5$**), and 481 nm (**PO$_6$**), respectively. It is noteworthy that the **PO$_2$** possesses a relatively broader, more intense, and redshifted absorption band as compared to the other dyes. The aforesaid shift is quite desirable as it hints at an improved light-harvesting ability in the devices. In addition, the molar extinction coefficients ($\boldsymbol{\varepsilon}$) of all the molecules **PO$_{1-6}$** were determined according to Lambert-Beer law (the detailed procedure is given in the ESI).[37,38] The $\boldsymbol{\varepsilon}$ values are found to be in the decreasing order, *i.e.* **PO$_2$** > **PO$_1$** > **PO$_6$** > **PO$_3$** > **PO$_5$** > **PO$_4$**. The shapes of the absorption bands are different for all the molecules demonstrating that the electron-withdrawing capacity of different acceptor units has a major effect on the absorption maxima as well as molar extinction coefficients. Among all the molecules, **PO$_2$** displays a higher molar extinction coefficient hinting at their good light-harvesting capability.

Further, the fluorescence emission spectra of molecules **PO$_{1-6}$** were recorded upon excitation at their absorbance maximum wavelengths in 10^{-5} M chloroform solutions. The normalized emission spectra are given in Figures 2b, 2c, and 2d show the emission behavior of synthesized molecules **PO$_{1-6}$** in 10^{-5} M chloroform solution under naked eyes (visible spectrum) and 360 nm UV light respectively. The fluorescence emission spectra of all the dyes display a single emission band in the range of 560-650 nm. The largest emission wavelength was detected at 649 nm for molecule **PO$_2$**, consistent with the absorption data and the strong electron-withdrawing nature of 1,3-diethyl-2-thiobarbituric acid. The Stokes

shift values of all the synthesized molecules were calculated by measuring the difference between absorption and emission maxima.[39] The Stokes shifts are rather similar and ranks as **PO3** (2520 cm^{-1}) < **PO4** (3100 cm^{-1}) < **PO6** < (3210 cm^{-1}) < **PO5** (3350 cm^{-1}), < **PO1** (3440 cm^{-1}) < **PO2** (3780 cm^{-1}). This large Stokes shifts are consistent with ICT band within these series of dyes, with the highest charge transfer transition on **PO2** and **PO1**. Furthermore, the optical 0-0 gap was calculated from the intersection of normalized absorption and emission spectral data and are found to be in the decreasing order, 2.40 eV (**PO1**) > 2.38 eV (**PO2**) > 2.31 eV (**PO3**) > 2.27 eV (**PO6**) > 2.19 eV (**PO5**) > 2.05 eV (**PO4**).

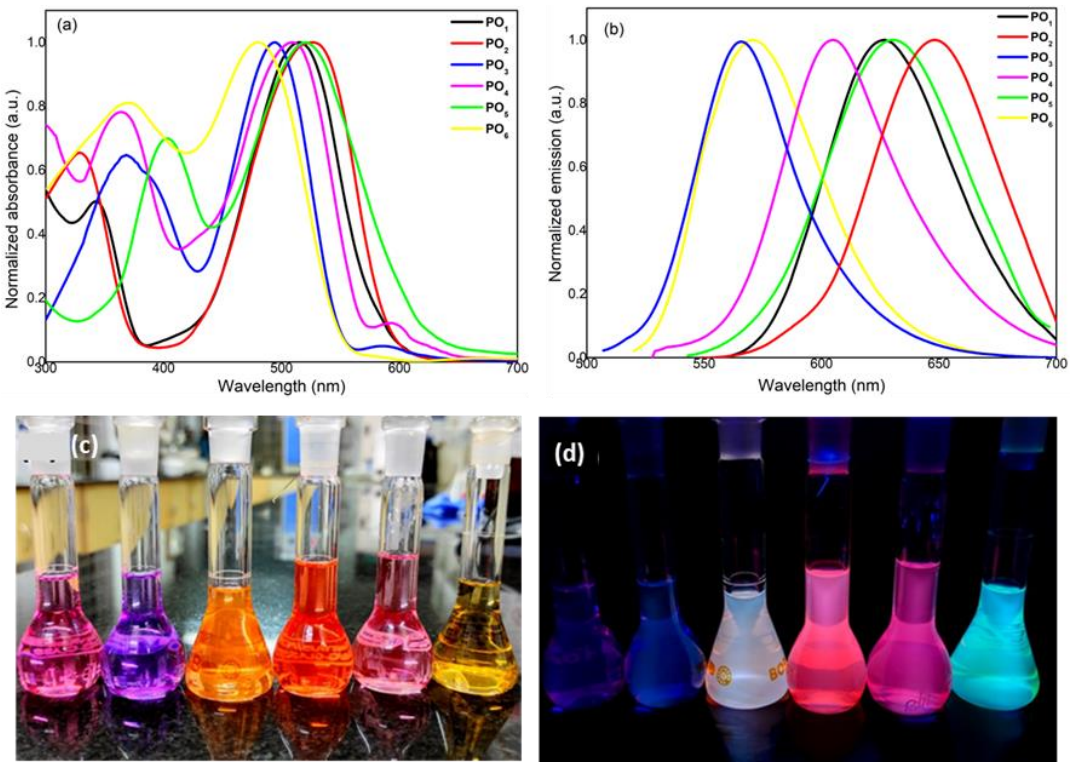

Figure 2. (a) Normalized UV-Vis absorption, (**b**) fluorescence emission spectra of **PO1-6** recorded in 10^{-5} M $CHCl_3$ solution, **(c)** pictures of the dye solutions under visible spectrum, and **(d)** pictures of the dye solutions irradiated with UV light at 360 nm

Table 1. Photophysical characterization data of **PO1-6**

Compound	λ_{abs} (nm)	λ_{emi} (nm)	Stokes shift (cm^{-1})	ε ($M^{-1}cm^{-1}$) at λ_{abs} (nm)	$E_{0\text{-}0\ opt}$ (eV)
PO1	515	626	3440	49500	2.40
PO2	521	649	3780	55200	2.38
PO3	496	567	2520	34500	2.31
PO4	510	606	3100	31100	2.05
PO5	518	628	3350	33700	2.19

PO$_6$	481	569	3210	36500	2.27

In order to obtain deeper insights into the ICT phenomenon inside the molecules, the solvatochromic behavior of **PO$_{1-6}$** in a variety of solvents with varying polarities was studied. Both absorption and emission spectra of all the synthesized molecules were determined in five different solvents, namely, tetrahydrofuran (THF), dichloromethane (DCM), ethyl acetate (EtOAc), *N*,*N*-dimethylformamide (DMF), and acetonitrile (ACN) at a concentration of 10^{-5} M at room temperature. Figures 3a-f display the solvatochromic absorption spectra of **PO$_{1-6}$** in this set of solvents starting from relatively non-polar solvent THF to highly polar DMF and acetonitrile at micro-molar concentration and the corresponding results are tabulated in Table 2.

As seen in the spectra, with the increasing solvent polarity there are small variations of the absorption behaviour of **PO$_{1-6}$**, but a clear trend to redshift in the more polar medium. This positive solvatochromism indicates an increase of the dipole moment when going from the ground to the excited state, as expected. This is also consistent with the theoretical calculations. In particular, the molecule **PO$_2$** (563 nm) exhibits the largest positive solvatochromic characteristics in all the solvents, particularly in the highest polar acetonitrile when compared to the other molecules. From Figures 3a-f, it is noticed that all the molecules manifested a slight hypsochromic shift in solvents such as THF, DCM, with a lower polarity than that of $CHCl_3$, whereas a minor bathochromic shift was observed in polar solvents such as EtOAc, DMF, and acetonitrile. The observed positive solvatochromism indicates that the excited state (ES) is more polar than the ground state (GS). In other words, the ES is more stable in polar solvents than GS and thus requires lower energy for the ES population from GS, which leads to a bathochromic shift of the absorption spectrum. This redshift in polar solvents arises from the effective solvation of the molecules, induced by the instant stabilization of polarizable electrons during the electronic excitation. Such behaviour is characteristic of the donor-acceptor conjugated systems. From the results, it is quite clear that there exists a prominent intramolecular charge transfer from the donor groups to electron acceptor units in the excited state of the molecules, demonstrating **PO$_{1-6}$** exhibit a polar excited state with a significantly increased dipole moment.

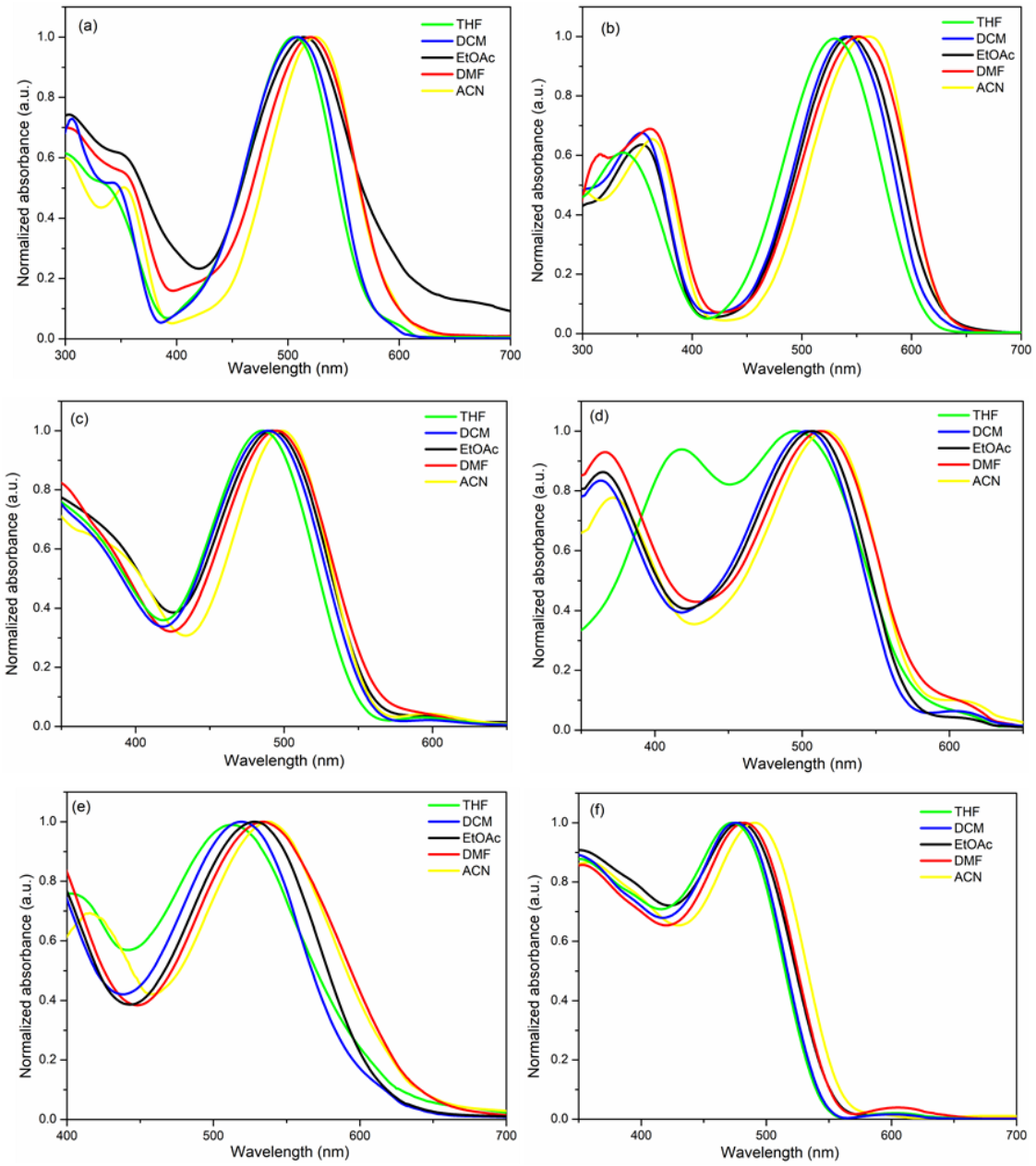

Figure 3. Normalized UV-Vis absorption spectra of **(a) PO_1**, **(b) PO_2**, **(c) PO_3**, **(d) PO_4**, **(e) PO_5**, and **(f) PO_6** in solvents with varying polarity index

Figures 4a-f displays the fluorescence emission spectra of molecules **PO_{1-6}** in the same six different solvents. One notices significant changes in the emission maxima as the solvent becomes more polar, again with the largest effect obtained for molecule **PO_2** (665 nm) which displays a higher emission wavelength compared to all other molecules. The enhanced emission in **PO_2** is likely due to the presence of a stronger electron-withdrawing moiety on the phenoxazine core. The Stokes shift values of **PO_{1-6}** in all the five solvents were calculated and the corresponding results are tabulated in Table 2. The results demonstrate that

all the molecules exhibit satisfactory positive solvatochromism and thus, all the molecules can be used as a potential light-harvester in DSSCs.

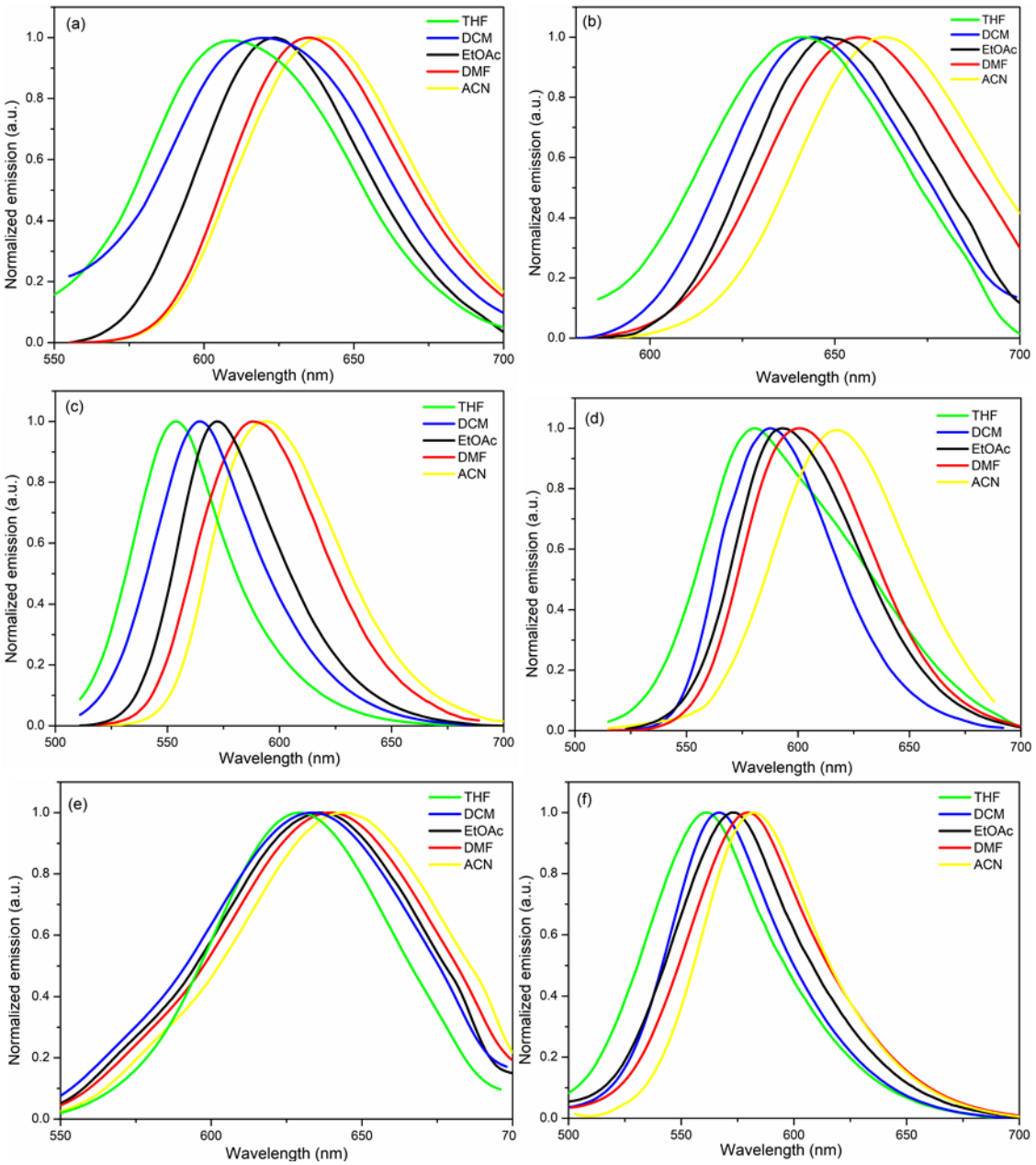

Figure 4. Normalized emission spectra of **(a) PO_1**, **(b) PO_2**, **(c) PO_3**, **(d) PO_4**, **(e) PO_5**, and **(f) PO_6** in solvents with varying polarity index

Table 2. Solvatochromic data of molecules **PO_{1-6}**

Molecules	**Parameters**	**THF**	**DCM**	**EtOAc**	**DMF**	**Acetonitrile**
	f (ε,n)	0.210	0.217	0.228	0.276	0.305
PO_1	$\lambda_{abs}{}^{a}$ (nm)	507	511	518	523	528
	$\lambda_{emi}{}^{b}$(nm)	610	622	627	636	640

	Stokes shift (cm^{-1})	3330	3490	3350	3390	3310
PO2	λ_{abs}[a] (nm)	529	540	545	553	563
	λ_{emi}[b](nm)	642	646	652	658	665
	Stokes shift (cm^{-1})	3320	3030	3010	2880	2720
PO3	λ_{abs}[a] (nm)	484	489	491	495	500
	λ_{emi}[b](nm)	554	566	572	588	595
	Stokes shift (cm^{-1})	2610	2780	2880	3190	3190
PO4	λ_{abs}[a] (nm)	497	504	507	513	518
	λ_{emi}[b](nm)	577	581	590	599	616
	Stokes shift (cm^{-1})	2780	2620	2770	2790	3070
PO5	λ_{abs}[a] (nm)	512	520	528	534	538
	λ_{emi}[b](nm)	625	630	634	640	644
	Stokes shift (cm^{-1})	3530	3350	3160	3100	3050
PO6	λ_{abs}[a] (nm)	475	481	483	487	493
	λ_{emi}[b](nm)	561	568	573	579	584
	Stokes shift (cm^{-1})	3220	3180	3250	3260	3160

[a] Absorption spectra measured in various solvents (concentration of 10^{-5} M)
[b] Emission spectra measured in various solvents (concentration of 10^{-5} M)

Theoretical studies

To obtain additional information regarding the nature of the excited states of dyes **PO1-6** TD-DFT calculations have been performed at the CAM-B3LYP/6-311+G(2d,p) level applying the cLR^2-PCM solvation model (see the ESI for computational details).[40] First, as can be seen in the EDD plots of Figure 5, the lowest excited state indeed presents an ICT nature, with the phenoxazine moiety acting as the donor (mostly in blue), the added pulling groups as the acceptor (mostly in red). In all compounds, the anchoring group does not play any direct role in the excited state. The topology of the EDD plots is similar in all cases, but for **PO5** in which the extended accepting unit induces a strong ICT (see also below), but the depletion of density is further from the anchoring group, *i.e.*, further from the surface of the semi-conductor, which might be detrimental in DSSC applications. In contrast, **PO6** obviously shows a smaller ICT than the other five dyes.

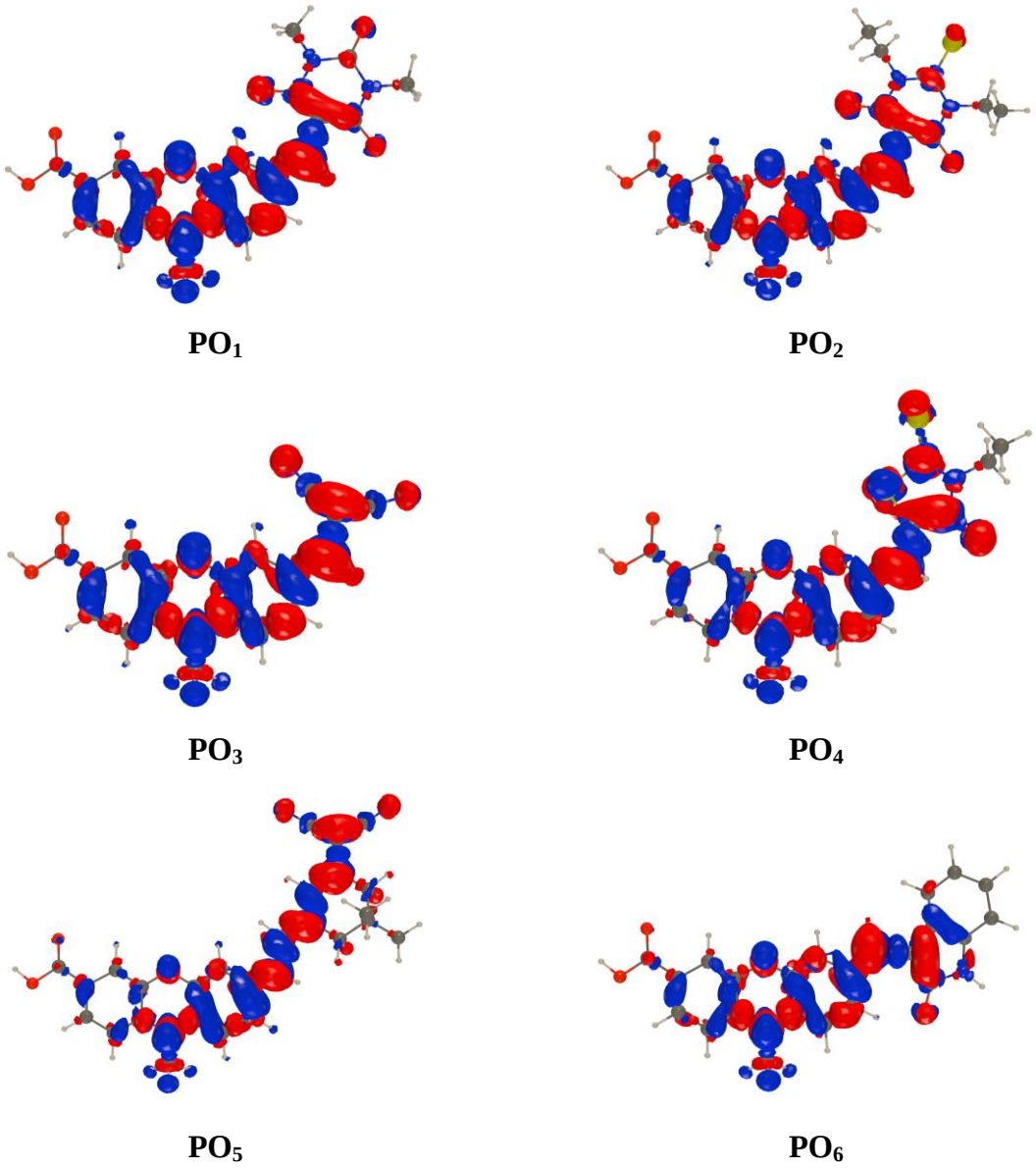

Figure 5. Electron density difference (EDD) plots corresponding to the lowest transition of all dyes. The blue and red lobes represent regions of decrease and increase of density upon absorption, respectively. Contour threshold: 0.001 au.

To obtain more quantitative data, we report in Table 3 theoretically computed data. One notes that the vertical absorption energy is blue-shifted as compared to the experimental λ_{max}, which is the expected trend in such a comparison. Nevertheless, except for **PO5** the ordering of the values matches the one of Table 1. Also consistent with the experiment is that large oscillator strength is computed for all compounds, indicative of intense bright transitions. We have also evaluated the ICT parameters. According to the calculations, photon absorption induces a charge separation of ca. 0.6 e over distances ranging from 2.3 Å (**PO6**) to 4.1 Å (**PO5**). Such values are indicative of large yet not huge ICT. Consistent with

this, one notices a strong increase of the dipole moments upon photon absorption, the two dyes undergoing the largest increase being **PO2** (+8.5 D) and **PO5** (+10.8 D), which is rather consistent with the solvatochromic study discussed above. Eventually, we have also used theory to determine 0-0 energies that can be more directly compared to the experiment than vertical transition energies. The values listed in Table 3 show that our 0-0 energies are comparable to the experimental values.

Table 3. TD-DFT determined data for **PO1-6**. We report the vertical absorption, related oscillator strength, the ICT parameters (ICT distance and amount of charge transferred), as well as the computed ground and excited state dipole moments.

Compound	λ_{vert} (nm)	*f*	$E_{0\text{-}0}$ (eV)	d^{CT}_i (Å)	q^{CT}_i (e)	μ_{GS} (D)	μ_{ES} (D)
PO1	445	0.81	2.54	2.90	0.63	9.2	16.7
PO2	467	0.97	2.43	3.12	0.64	11.0	19.5
PO3	439	0.72	2.58	2.74	0.60	14.8	21.3
PO4	440	0.96	2.60	2.96	0.63	10.4	17.8
PO5	479	1.48	2.38	4.10	0.67	18.2	29.0
PO6	429	1.00	2.54	2.25	0.56	3.2	7.3

Thermal properties

The thermal characteristics of the dyes **PO1-6** were studied by thermogravimetric analyses (TGA) at the heating rate of 10 °C min^{-1} under a nitrogen atmosphere. The TGA plots of molecules **PO1-6** are shown in Figure 6. All the synthesized dyes exhibit satisfactory thermal stability with high thermal decomposition (T_d) temperatures at 392 °C (**PO1**), 408 °C (**PO2**), 362 °C (**PO3**), 278 °C (**PO4**), 289 °C (**PO5**), and 336 °C (**PO6**). Among all, the chromophores **PO1** and **PO2** carrying barbituric acid derivatives as an electron-acceptor unit are those presenting the highest thermal stability, suggesting good stability of the devices if applied as sensitizers.

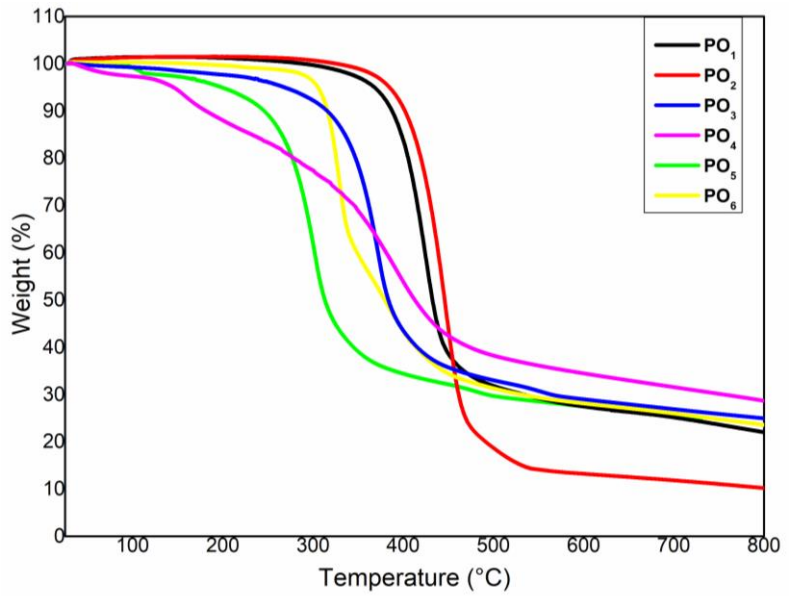

Figure 6. TGA thermograms of **PO1-6** obtained at a heating rate of 10 °C min^{-1} under nitrogen atmosphere

Electrochemical properties

The thermodynamic feasibility of the hole injection from the photoexcited dyes into the valence band (VB) of semiconductor NiO and the electron transfer from the reduced dye molecule to the redox couple in the electrolyte can be effectively demonstrated using redox potentials determined by cyclic voltammetry (CV). The experiments are performed using a conventional three-electrode system, in which platinum disc, glassy carbon, and Ag/AgCl serve as passive, working, and reference electrodes, respectively.[41,42] The generated voltammograms of **PO1-6** are depicted in Figure S36 and a pictorial representation of their energy level diagram is given in Figure 7. The reduction potentials of the excited state (E_{Red}^{*}) of **PO1-6**, as estimated from the difference between reduction potential (E_{Red}) and optical band gap ($E_{0\text{-}0}$), are in the range of 1.3 to 1.6 V *vs.* SCE, which is much more positive than the valence band of NiO (E_{VB}(NiO) = 0.3 V *vs.* SCE) guaranteeing a large driving force for hole injection (about –1.4 eV) from the dye excited state to the NiO valence band (Figure 7 and Table 4). This is an interesting feature for the application of these dyes with *p*-type semiconductors that have a deep valence band potential, such as $PbTiO_3$, and require thus strongly oxidizing sensitizers.[43] The reduction potentials (approximately the LUMO energy levels) of the molecules, ranging from –0.66 to –0.80 V *vs.* SCE, are sufficiently negative to ensure a significant driving force for regeneration with the iodide/triiodide redox mediator (Table 4). Thus, all the dyes exhibit suitable energy levels for adequate thermodynamic driving forces which are mandatory for the charge transfer steps occurring smoothly in p-

DSSC. Indeed, the thermodynamic feasibilities of hole injection from the dye and regeneration processes of **PO1-6**, quantitatively given by the Gibbs free energies of those processes (ΔG_{inj} and ΔG_{reg}), were estimated using equations (1) to (2) and the corresponding data are given in Table 4. The energy levels were efficiently tuned by varying electron acceptor units, and thus it has a large influence on the hole injection as well as the dye regeneration mechanism. The Gibbs free energy to inject a hole from the excited state of the dye into the VB edge of the NiO semiconductor was estimated from equation 1.

$$\Delta G_{inj} = E_{VB}(NiO) - E^*_{Red} \qquad (1)$$

Here, ΔG_{inj} is the Gibbs free energy for injection, E^*_{Red} is the reduction potential of the dye in its excited state and E_{VB} (NiO) is the Nernst potential of the VB of NiO, *i.e.* 0.30 V *vs.* SCE.

Furthermore, the Gibbs free energy for dye regeneration from electrolyte (ΔG_{reg}) was estimated from the difference between the reduction potential of the dye and Nernst potential of I_3^-/I^- electrolyte system (–0.32 V *vs.* SCE) and it can be expressed as equation 2

$$\Delta G_{reg} = E_{Red} - E_{I_3^-/I_2^-} \qquad (2)$$

The ΔG_{inj} values are in the order, **PO2** (–1.37 eV) ≈ **PO3** (–1.36 eV) > **PO1** (–1.30 eV) ≈ **PO6** (–1.29 eV), > **PO5** (–1.23 eV) > **PO4** (–1.01 eV) whereas ΔG_{reg} values of dyes are in the order, **PO1** (–0.48 eV) > **PO4** (–0.42 eV) > **PO2** (–0.39 eV) > **PO6** (–0.36 eV) ≈ **PO5** (–0.34 eV) ≈ **PO3** (–0.33 eV). **PO1** features the largest dye regeneration driving force with a common redox mediator. As expected, the nature of the electron acceptor significantly influences the LUMO level of the dye molecule, a stronger electron-withdrawing ability corresponding to a lower lying LUMO level. Thus, dye **PO2** may result in little lower thermodynamic driving force for dye regeneration as compared to **PO1** and **PO4**. However, the presence of strong electron acceptor unit will improve the push-pull nature of the dye molecule, which ultimately enhances the efficiency of charge separation within the molecule. Conclusively, the electrochemical studies revealed that all the *p*-type organic chromophores (**PO1-6**) fulfilled the prerequisites for effective electron injection and dye regeneration processes in the fabricated devices.

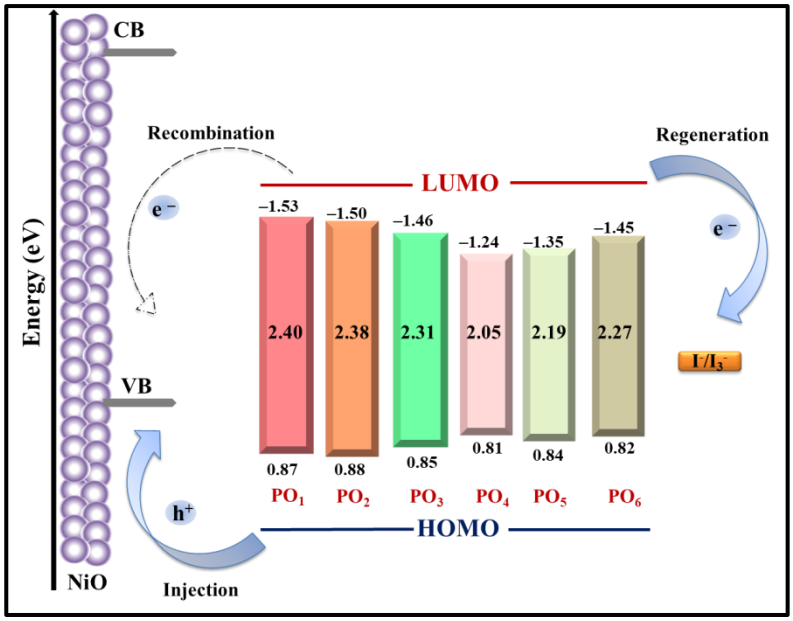

Figure 7. Molecular energy level diagram showing experimental HOMO, LUMO, of **PO1-6** and position of NiO valence band along with the redox potential of the iodide/triiodide redox mediator

Table 4. Electrochemical properties of *p*-type organic chromophores **PO1-6**. All the potentials are referenced *versus* saturated calomel electrode (SCE).

Compound	E_{Red} (V)	E_{Red}^{*} (V)	ΔG_{inj} (eV)	ΔG_{reg} (eV)
PO1	–0.80	1.60	–1.30	–0.48
PO2	–0.71	1.67	–1.37	–0.39
PO3	–0.65	1.66	–1.36	–0.33
PO4	–0.74	1.31	–1.01	–0.42
PO5	–0.66	1.53	–1.23	–0.34
PO6	–0.68	1.59	–1.29	–0.36

The E* values were formulated by, $E_{Red}^{*} = E_{Red} + E_{0\text{-}0}$. $\Delta G_{inj} = E_{VB}$ (NiO) – E_{Red}^{*} (dye*/dye^{-}) with E_{VB} (NiO) = 0.30 V *vs.* SCE. $\Delta G_{reg} = E_{Red}$ (dye/dye^{-}) – E ($I_3^{-}/I_2^{-\bullet}$) with E($I_3^{-}/I_2^{-\bullet}$) = –0.32 V *vs.* SCE (Boschloo et al., 2011; Farré et al., 2016; Black et al., 2017).

Photovoltaic studies

Finally, the sensitizers **PO1-6** along with the benchmark reference dye 4-(bis-{4-[5-(2,2-dicyanovinyl)-thiophene-2-yl]-phenyl}amino)benzoic acid (**P1**) were tested on nanocrystalline NiO-based photocathodes using the iodide/triiodide couple as redox shuttle (see the experimental part for details). The short circuit photocurrent density (J_{SC}), open-circuit voltage (V_{OC}), fill factor (*FF*), and photoconversion efficiency (*PCE*) recorded under

stimulated AM1.5G solar light (100 $mW \cdot cm^{-2}$) are listed in Table 5. The action spectra of the incident photon-to-current conversion efficiency (*IPCE*) as a function of the incident wavelength of the *p*-DSSCs and the current/voltage characteristics are respectively shown in Figure 8 and Figure S37.

Amongst the tested dyes, the photovoltaic performances were found to be ordered as **P1** > **PO$_2$** ≈ **PO$_1$** > **PO$_6$** ≈ **PO$_3$** > **PO$_5$** >> **PO$_4$**. All these dyes are less efficient than the benchmark reference **P1**. This could be due to a lower hole injection efficiency as the HOMO does not spread on the anchoring group (Figure 5) reducing thus the electronic coupling with the valence band of NiO. Another distinct feature of **P1** with these dyes is its branched structure with two electron-accepting units, that can: i) dilute the electron density and thus retard charge recombination and ii) shield the NiO surface preventing the redox mediator from its physical approach to the surface. A denser packing on the surface is favourable, particularly with *p*-DSSC as it decreases interfacial charge recombination. Except for **PO$_2$**, which gives the highest *Voc*, the differences in the photovoltaic performance of **PO$_{1\text{-}6}$** are mainly due to the photocurrent density, with the highest value recorded for **PO$_6$**. Interestingly, **PO$_4$** has surprisingly much lower PV performances than the other dyes featuring a particularly low V_{OC} and *FF*, which could be tentatively attributed to higher charge recombination stemming from a different organization on the NiO surface. Indeed, as far as the exergonicities of charge transfer are concerned, they are not very distinct from the other dyes (Table 4), but the solvatochromism study indicates a higher tendency to form aggregates. This deleterious process likely takes place after chemisorption on NiO surface and alters charge injection and favours interfacial charge recombination with the electrolyte or the geminate charge recombination.[44,45] To shed some light on this parameter, a series of solar cells were prepared with the dyes chemisorbed in presence of 5 mM of chenodeoxycholic acid (CDCA) in the dye bath (Table S1). Overall, we observed that the presence of CDCA in the dye bath does not importantly improve the photovoltaic performances ruling out that aggregation is the main cause of the modest *PCEs*. With the majority of the dyes such as **PO$_1$**, **PO$_3$**, **PO$_4$**, **PO$_5$**, and **PO$_6$** the addition of CDCA diminishes the *PCE* (by *circa* 10%), due to a decrease of J_{SC}, which is certainly ascribed to a lower light-harvesting efficiency; the other characteristics (V_{OC} and FF) remain constant within experimental error. For dye **PO$_2$**, the J_{SC} is slightly enhanced in presence of CDCA (about 10%), resulting in a negligible *PCE* change. Then, to determine the impact of dye loading, they were measured by desorption experiments using phenyl phosphonic acid as a competitor, since the presence of strongly electron-withdrawing groups on these dyes makes

them prone to degradation using classical hydroxide solution (Table S2).[46] These milder desorption conditions enable the determination of the dye loading of all the dyes except that of **PO2** and **PO4** which degrade in presence of a high concentration of phenyl phosphonic acid, as proved by the strong colour change of the final solution. The dye loading is ranked in the following order: **PO5** > **PO1** ≈ **PO6** > **PO3** with no real relationship with the *PCE*, which is consistent with the negligible impact of CDCA, since aggregation plays a minor role in the performances. It was observed in TiO_2 based DSSC, that lateral charge diffusion by hole hopping between the dyes (which is assisted by a close packing), increases the geminate charge recombination. As a result, the facilitated electron hopping between the dyes could also increase the charge recombination in *p*-DSSC with this dye. The larger *Voc* of **PO2** could be explained by either lower charge recombination or its larger dipolar moment, which downward bends the VB of NiO. The latter hypothesis is ruled out by the calculated dipole moments (Table 3). The dark current is found to be lower in **PO2** than other dyes, indicating a decrease of the interfacial charge recombination with the electrolyte probably related to a denser packing on the NiO surface. However, J_{SC} of dye **PO2** is found to be lower when compared to the device fabricated using dye **PO6** suggesting a weaker hole injection efficiency owing to a lower electronic coupling. From these results, it can be concluded that the performance of the device sensitized with **PO1-6** may be influenced substantially by minor structural alterations.

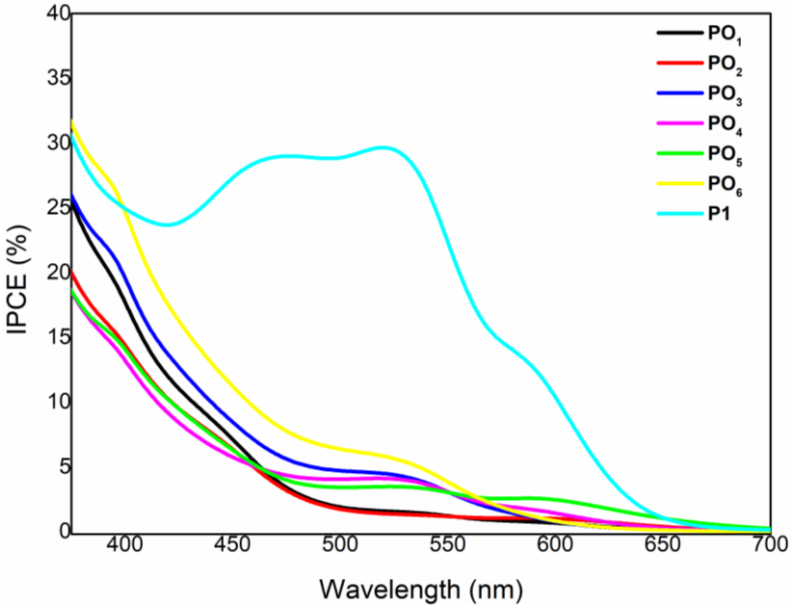

Figure 8. *IPCE* spectra of DSSCs sensitized with dyes **PO1-6** under illumination of simulated solar light (AM 1.5G, 100 $mW{\cdot}cm^{-2}$).

Table 5. Photovoltaic performance data of devices sensitized with *p*-type dyes (**PO1-6**) recorded on simulated AM1.5 (100 W·m^{-2}).

Sensitizer	J_{SC} (mA·cm^{-2})	V_{OC} (mV)	*FF* (%)	*PCE* (%)
P1	3.55± 0.2	115 ± 10	31 ± 3	0.126 ± 0.06
PO1	1.05 ± 0.03	89 ± 2	33 ± 1	0.030 ± 0.01
PO2	0.89 ± 0.08	101 ± 5	35 ± 1	0.031 ± 0.01
PO3	1.06 ± 0.03	79 ± 5	32 ± 1	0.026 ± 0.01
PO4	0.77 ± 0.06	32 ± 2	25 ± 3	0.006 ± 0.02
PO5	0.98 ± 0.1	79 ± 5	31 ± 3	0.024 ± 0.02
PO6	1.25 ± 0.2	72 ± 5	32 ± 3	0.027 ± 0.03

Conclusions

In summary, we designed and synthesized six new push-pull phenoxazine-based organic chromophores, **PO1-6**, comprising different acceptor units for *p*-DSSC applications. To the best of our knowledge, this is the first time that phenoxazine core has been used as an electron donor unit in D-A type dyes designed for *p*-type DSSCs. Based on their joint theoretical, optical, thermal, and electrochemical studies, dyes **PO1-6** were shown to possess all the prerequisites to act as a potential sensitizer in the devices. Accordingly, the devices were fabricated by employing them as a sensitizer and their device performance parameters were evaluated with emphasis on the structure-performance correlation studies. Amongst **PO1-6**, the dye carrying *N*,*N*-diethyl thiobarbituric acid as an electron acceptor (**PO2**) displayed the highest *PCE* of 0.031 % (J_{SC}: 0.89 mA·cm^{-2}, V_{OC}: 101 mV, and *FF*: 35 %). The superiority of **PO2** can be assigned to the presence of a strong electron acceptor unit. By varying electron acceptor units, the energy levels of the sensitizers can be efficiently tuned, and hence, it has a large influence on the hole injection as well as the dye regeneration mechanism. Thus, we trust that this work contributes to a better molecular design strategy of organic dyes to further ameliorate the performance of *p*-type DSSCs.

Experimental Section

Materials and methods

The starting materials such as 10*H*-phenoxazine, 2-ethylhexyl bromide, *N*,*N*-dimethyl barbituric acid, *N*,*N*-diethyl thiobarbituric acid, malononitrile, 3-ethylrhodanine, (3,5,5-trimethylcyclohex-2-enylidene)malononitrile, and *2*-oxindole were procured from Sigma-Aldrich and Alfa Aesar companies. All the solvents used in the reactions were of synthetic grade (Merck, Loba Chemie, and Spectrochem companies) and they were purified by further drying and distillation process. All the reactions were carried under an inert (argon) atmosphere and the reaction completion was monitored by the TLC technique. The designed dyes were synthesized by using standard synthesis protocols. The target dyes and their intermediates were purified using recrystallization or column chromatographic separation techniques. The melting points of synthesized molecules were recorded using the Stuart SMP10 digital melting point apparatus.^{1}H NMR (400 MHz) spectra of synthesized molecules were recorded on the Bruker Avance (III) 400 MHz instrument by using $CDCl_3$/DMSO-d_6 as a solvent. The chemical shift (δ) was expressed in parts per million (ppm) relative to the solvent residual peak with tetramethylsilane (TMS) as an internal standard and coupling constant (J) is expressed in Hz. The LCMS and elemental analysis of the synthesized dyes **PO$_{1-6}$** were obtained from the LC-MS6410Q (Agilent Technologies) and Flash EA1112 CHNS elemental analyzer (Thermo Scientific), respectively. FT-IR spectra were obtained using the Bruker FTIR Alpha spectrometer. Also, Thermogravimetric analysis (TGA) was carried out using the Perkin Elmer TGA4000 analyzer, at the heating rate of 10 °C min^{-1} under the nitrogen atmosphere. The UV-Vis absorption spectra and photoluminescence spectra of **PO$_{1-6}$** in various solvents were recorded at room temperature by using the Analytik Jena SPECORD S 600 and Jasco FP 6200 spectrophotometers, respectively. Furthermore, in order to assess their experimental GSOP and ESOP values, the CV (cyclic voltammetry) measurements were performed in anhydrous acetonitrile solution with 0.1M tetrabutylammonium hexafluorophosphate [TBA] [PF_6] as a supporting electrolyte at a scan rate of 100 mVs^{-1}. In the CV experiments, the cyclic voltammograms were recorded at the applied voltage of +2 to –2 V.

Photoelectrochemical measurements

For device fabrication studies, the conductive glass substrates (F-doped SnO2) were purchased from Solaronix (TEC15, sheet resistance 15 Ω/square). A set-up comprising Oriel

solar simulator (AM 1.5G, 100 $mW \cdot cm^{-2}$) calibrated with a silicon cell covered with KG5 filter and attached to Keithley 2400 digital source meter was used for measuring photovoltaic parameters. IPCE experiments were carried out for the fabricated devices using ZAHNER's CIMPS-QE/IPCE system.

Theoretical calculations

We have performed all calculations with Gaussian16.A.03[47] replacing the long alkyl chain of the phenoxazine by a methyl group for obvious computational reasons. The ground-state geometries were optimized at PBE0[48]/6-311G(d,p) level taking into account solvation effects using the well-known PCM[49] model, selecting $CHCl_3$ as solvent. It was systematically checked that these structures are stable for computation of the vibrational frequencies. We performed a conformational search for the side accepting units starting with chemically-intuitive conformations and report only the most stable structures. We next used TD-DFT on these structures to characterize the excited states and more precisely selected a CAM-B3LYP[50]/6-311+G(2d,p) approach combined with the cLR^2 solvation model that includes both linear-response and state-specific effects.[51] These choices of functional and solvent models were dictated by the nature of the investigated excited states (bright with ICT character). The ICT parameters were determined with the same functional and basis set using Le Bahers' model.[52] The 0-0 energies were determined thanks to TD-DFT optimization of the excited-state structures, followed by calculations of the vibrational energies and of the vertical fluorescence, using exactly the same methods as for the absorption, i.e., PBE0/6-311G(d,p) for structural and vibrational parameters and CAM-B3LYP/6-311+G(2d,p) for transition energies.

Synthetic methods

*Synthesis of 10-(2-ethylhexyl)-10H-phenoxazine (**1**)*

A mixture of phenoxazine (0.5 g, 2.72 mmol), NaH (1.9 g, 8.16 mmol) was dissolved in a minimum amount of DMF (8 mL) and stirred at room temperature for half an hour under an inert atmosphere. Later, 2-ethylhexyl bromide (0.58 mL, 3.27 mmol) was added into the reaction mixture and continued stirring at room temperature for 12 h. The reaction progress was monitored using TLC. After completion of the reaction, the reaction mixture was cooled and poured into crushed ice (100 mL) and neutralization was done using a saturated solution of ammonium chloride. The residue formed was extracted with ethyl acetate (50 mL x 4) and the organic layer was dried over sodium sulphate and evaporated under reduced pressure. The

impure residue was later purified by column chromatography on silica gel (100-200 mesh and hexane: EtOAc eluent) to yield a colorless liquid as a product. Yield: 97%.

^{1}H NMR (400 MHz, $CDCl_3$, δ ppm): 6.77-6.73 (m, 2H), 6.61-6.60 (d, 4H), 6.51-6.49 (m, 2H), 3.39-3.37 (d, 2H), 1.88-1.85 (m, 1H), 1.36-1.29 (m, 8H), 0.90-0.87 (t, 6H). Anal. Calcd. for $C_{20}H_{25}NO$: C, 81.31; H, 8.53; N, 4.74; and found C, 80.89; H, 8.29; N, 4.06.

*Synthesis of 10-(2-ethylhexyl)-10H-phenoxazine-3-carbaldehyde (**2**)*

In a cleaned RB flask, freshly distilled DMF (0.13 mL, 1.69 mmol) was taken and cooled at –3 to 4 ºC. Then, phosphorous oxychloride, $POCl_3$ (0.09 mL, 1.01 mmol) was added drop-wise with constant stirring at the same temperature under argon atmosphere to obtain a glassy white salt. To this mixture, 10-(2-ethylhexyl)-10*H*-phenoxazine (**1,** 0.1 g, 0.33 mmol) dissolved in dichloroethane (2 mL) was added. The reaction mixture was refluxed at 95 ºC for 12 h. After completion of the reaction, the reaction mass was cooled to room temperature and poured into 100 mL crushed ice, and subsequently basified by using a 5 M NaOH solution. The product formed was extracted with ethyl acetate (50 mL x 3) and the organic layer was dried over sodium sulphate and evaporated under reduced pressure. The impure residue was later purified by column chromatography on silica gel (100-200 mesh) to yield a light brown solid (**2**). Yield: 79 %. Melting point: 112-114 °C.

^{1}H NMR (400 MHz, $CDCl_3$, δ ppm): 9.68 (s, 1H), 7.32-7.30 (m, 1H), 7.10-7.09 (d, 1H), 6.83-6.80 (m, 1H), 6.75-6.74 (d, 1H), 6.68-6.66 (d, 1H), 6.61-6.58 (t, 1H), 3.50-3.48 (d, 2H), 1.92-1.89 (m, 1H), 1.50-1.31 (m, 8H), 0.97-0.94 (t, 3H), 0.92-0.89 (t, 3H). **^{13}C NMR** (400 MHz, $CDCl_3$, δ ppm): 189.63, 145.18, 144.77, 140.16, 132.09, 129.80, 128.43, 123.70, 122.55, 115.84, 114.41, 112.82, 111.23, 47.77, 36.64, 30.68, 28.75, 24.10, 23.07, 14.03, 10.97. Anal. Calcd. for $C_{21}H_{25}NO_2$: C, 77.98; H, 7.79; N, 4.33; and found C, 77.90; H, 7.71; N, 4.23.

*Synthesis of 10-(2-ethylhexyl)-10H-phenoxazine-3-carboxylic acid (**3**)*

In a cleaned RB flask, sodium hydroxide (0.67 g, 17 mmol) was taken and slowly dissolved in 100 mL of ethanol by stirring under an ice bath. Further, the silver oxide (0.35 g, 1.54 mmol) was suspended in this solution and to this mixture 10-(2-ethylhexyl)-10*H*-phenoxazine-3-carbaldehyde (**2**, 0.1 g, O.309 mmol) dissolved in 10 mL of toluene solution was slowly added with constant stirring at RT. The stirring was continued for 16-18 h under

an argon atmosphere. After completion of the reaction, the reaction mixture was filtered through a celite bed. Further, the solvent of the filtrate was removed under vacuum and the obtained residue was washed with distilled water. The product was extracted with ethyl acetate (4 × 100 mL) and the organic phase was washed with 10 % sodium bicarbonate solution. Pre-cooled 10 % HCl was added to the collected aqueous layer and the pH of the solution was brought to slightly acidic. The precipitated solid was filtered and dried. The residue was purified using column chromatography on 200-400 mess silica using 2:1 hexane/ethyl acetate mixture as the mobile phase to get a pale-yellow solid. Yield: 77 %. Melting point: 138-140 ºC.

^{1}H NMR (400 MHz, $CDCl_3$, δ ppm): 9.72 (s, 1H), 7.61-7.59 (m, 1H), 7.36-7.28 (m, 3H), 7.13-7.12 (d, 1H), 6.67-6.61 (m, 2H), 3.55-3.54 (d, 2H), 1.91-1.89 (m, 1H), 1.51-1.33 (m, 8H), 0.99-0.95 (t, 3H), 0.93-0.89 (t, 3H). **^{13}C NMR** (400 MHz, $CDCl_3$, δ ppm): 189.70, 170.09, 145.17, 144.30, 138.59, 137.35, 130.93, 128.11, 127.08, 123.00, 117.02, 114.90, 112.14, 47.99, 36.64, 30.65, 28.72, 24.09, 23.03, 14.01, 10.95. Anal. Calcd. for $C_{21}H_{25}NO_3$: C, 74.31; H, 7.42; N, 4.13; and found C, 74.29; H, 7.41; N, 4.03.

*Synthesis of methyl 10-(2-ethylhexyl)-10H-phenoxazine-3-carboxylate (**4**)*

In a dry RB flask, 10-(2-ethylhexyl)-10*H*-phenoxazine-3-carboxylic acid (**3**, 1 g, 3.39 mmol) was dissolved in 15 mL of dry methanol and 2 drops of conc. H_2SO_4 was added. The reaction mixture was further refluxed for 3 h. After completion of the reaction, the product was cooled to RT and the solvent methanol was removed under vacuum using a rota evaporator. The residue was extracted with ethyl acetate (3 × 30 mL) and the organic layer was washed with a 10 % sodium carbonate solution, followed by water. Then, it was dried using sodium sulfate and the solvent was removed under vacuum to get a pale-yellow liquid. Yield: 90 %.

^{1}H NMR (400 MHz, $CDCl_3$, δ ppm): 7.51-7.49 (m, 1H), 7.24-7.24 (d, 1H), 6.82-6.78 (m, 1H), 6.71-6.69 (m, 1H), 6.65-6.64 (d, 1H), 6.57-6.55 (d, 1H), 6.51-6.49 (d, 1H), 3.86 (s, 3H), 3.45-3.43 (d, 2H), 1.90-1.87 (m, 1H), 1.33-1.32 (m, 8H), 0.96-0.91 (t, 6H). **^{13}C NMR** (400 MHz, $CDCl_3$, δ ppm): 166.35, 144.93, 144.43, 138.58, 132.72, 126.19, 123.58, 122.09, 121.94, 116.13, 115.66, 112.51, 111.08, 51.79, 47.63, 36.60, 30.70, 29.73, 28.76, 24.11, 23.08, 14.15, 14.04, 10.97. Anal. Calcd. for $C_{22}H_{27}NO_3$: C, 74.76; H, 7.70; N, 3.96; and found C, 74.25; H, 7.67; N, 3.88.

*Synthesis of methyl 10-(2-ethylhexyl)-7-formyl-10H-phenoxazine-3-carboxylate (**5**)*

In a cleaned dry RB flask, freshly distilled DMF (4.8 mL, 62.2 mmol), $POCl_3$ (5.8 mL, 62.2 mmol) was added slowly with constant stirring maintained at 0 ºC under an argon atmosphere. Then, a solution of methyl 10-(2-ethylhexyl)-10*H*-phenoxazine-3-carboxylate (**4**, 0.5 g, 1.41 mmol) dissolved in 5 mL of dichloroethane was added to the above reaction mixture with constant stirring. The reaction flask was allowed to attain room temperature and then heated at 90 ºC for 12 h. The reaction mass was quenched in ice-cold water. Its pH was adjusted to 1.0 by adding a 5 M sodium hydroxide solution. The solution was extracted with ethyl acetate (4 x 50 mL) and dried over anhydrous sodium sulfate. The solvent was removed under a vacuum to get a pale-orange liquid. Yield: 93 %.

^{1}H NMR (400 MHz, $CDCl_3$, δ ppm): 9.71(s, 1H), 7.54-7.52 (m, 1H), 7.34-7.28 (m, 2H), 7.12-7.11 (m, 1H), 6.65-6.59 (m, 2H), 2.94 (s, 1H), 3.53-3.51 (d, 2H), 1.91-1.87 (m, 1H), 1.42-1.30 (m, 8H), 0.97-0.94 (t, 3H), 0.92-0.88 (t, 3H). **^{13}C NMR** (400 MHz, $CDCl_3$, δ ppm): 189.63, 166.00, 145.15, 144.26, 138.77, 136.56, 130.78, 128.16, 126.22, 124.01, 116.57, 114.75, 112.10, 111.96, 51.99, 47.93, 36.63, 30.65, 28.72, 24.08, 23.02, 14.00, 10.94.

*Synthesis of 10-(2-ethylhexyl)-7-formyl-10H-phenoxazine-3-carboxylic acid (**6**)*

In a cleaned dry RB flask, the intermediate (**5**) was taken and dissolved in 10 mL of methanol. To this solution, 0.25 g of $LiOH.H_2O$ dissolved in 10 mL of water was added and stirred at 80 ºC for 8 h. Then, the methanol was removed and the solution was diluted with 100 mL of water. Further, the pH of the solution was made to just be acidic by adding pre-cooled 10 % HCl. The precipitated solid was filtered off and purified using column chromatography technique on 200-400 mess silica using 2:1 hexane/ethyl acetate mixture. Brown color solid, yield 62%. Melting point: 198-200 ºC.

^{1}H NMR (400 MHz, $CDCl_3$, δ ppm): 12.69 (s, 1H), 9.68 (s, 1H), 7.46-7.42 (m, 2H), 7.10-7.08 (d, 2H), 7.06-7.04 (d, 1H), 6.98-6.90 (m, 1H), 3.66-3.64 (d, 2H), 1.80-1.79 (m, 1H), 1.42-1.20 (m, 8H), 0.89-0.80 (t, 6H). **^{13}C NMR** (400 MHz, $CDCl_3$, δ ppm): 190.54, 166.83, 166.67, 166.60, 144.77, 144.41, 144.11, 144.02, 138.78, 138.44, 137.12, 136.51, 130.78, 128.85, 126.70, 124.82, 124.28, 116.06, 115.79, 114.28, 113.59, 113.46, 113.19, 36.27, 30.24, 30.14, 28.42, 23.70, 22.96, 14.24, 11.16. Anal. Calcd. for $C_{22}H_{25}NO_4$: C, 71.91; H, 6.86; N, 3.81; and found C, 71.90; H, 6.82; N, 3.79.

*General synthetic procedure for dyes **PO_{1-2}***

The starting material 10-(2-ethylhexyl)-7-formyl-10*H*-phenoxazine-3-carboxylic acid (**6**, 0.2 g, 0.54 mmol) was dissolved in 10 mL of absolute methanol and stirred at room temperature for 0.5 h. Then, respective clear solution of *N,N*-dimethyl barbituric acid (0.1 g, 0.65 mmol, 1.2 eq) or *N,N*-diethyl thiobarbituric acid (0.13 g, 0.65 mmol, 1.2 eq) dissolved in 5 mL of methanol was added to it slowly with constant stirring. Further, the reaction mass was stirred at 65 ºC for 10 h. The precipitated solid was filtered and washed with pre-cooled methanol. The obtained dyes were purified by column chromatography with a 2:1 hexane:ethyl acetate solvent system.

*7-((1,3-Dimethyl-2,4,6-trioxotetrahydropyrimidin-5(2H)-ylidene)methyl)-10-(2-ethylhexyl)-10H-phenoxazine-3-carboxylic acid (**PO$_1$**)*

Pinkish red solid, Yield 87 %. Melting point: 228-230 ºC. **^{1}H NMR** (400 MHz, DMSO-d6, δ ppm): 12.74 (s, 1H), 8.10-8.08 (d, 2H), 7.71-7.69 (d, 1H), 7.46-7.44 (d, 1H), 7.12 (s, 1H), 6.94-6.89 (m, 2H), 3.68-3.67 (d, 2H), 3.22 (s, 6H), 1.36-1.23 (m, 9H), 0.89-0.81 (t, 6H). **^{13}C NMR** (400 MHz, DMSO-d6, δ ppm): 166.54, 162.99, 161.30, 154.87, 151.41, 144.23, 143.23, 138.42, 136.22, 135.79, 126.45, 126.40, 125.22, 119.82, 116.00, 114.42, 113.79, 112.80, 47.32, 36.49, 31.15, 30.16, 29.07, 28.45, 23.73. Anal. Calcd. for $C_{28}H_{31}N_3O_6$: C, 66.52; H, 6.18; N, 8.31 and found C, 66.50; H, 6.11; N, 8.26. **FT-IR (ATR), υ** cm^{-1}: 2961 (C-H stretch), 1670 (C=O stretch), 1558, 1494 (C=C). **Mass (m/z):** Calculated: 505.56; Obtained (M-H): 504.25.

*7-((1,3-Diethyl-4,6-dioxo-2-thioxotetrahydropyrimidin-5(2H)-ylidene)methyl)-10-(2-ethylhexyl)-10H-phenoxazine-3-carboxylic acid (**PO$_2$**)*

Purple solid, Yield 87%. Melting point: 228-230 ºC. **^{1}H NMR** (400 MHz, DMSO-d6, δ ppm): 12.72 (s, 1H), 8.17-8.13 (m, 2H), 7.80-7.78 (d, 1H), 7.48-7.45 (m, 1H), 7.16 (s, 1H), 6.99-6.95 (m, 2H), 4.45-4.41 (q, 4H), 3.73-3.71 (d, 2H), 1.37-1.34 (m, 1H), 1.24-1.20 (m, 6H), 1.19-0.91 (m, 8H), 0.89-0.81 (t, 6H). **^{13}C NMR** (400 MHz, DMSO-d6, δ ppm): 178.89, 166.50, 161.27, 159.04, 156.95, 144.29, 144.02, 143.26, 139.36, 137.32, 136.52, 135.41, 126.70, 126.45, 125.62, 119.94, 116.09, 114.35, 114.08, 113.48, 112.96, 47.42, 43.91, 43.41, 36.55, 30.14, 28.44, 23.71, 22.98, 14.27, 12.68, 12.63, 11.19. Anal. Calcd. for $C_{30}H_{35}N_3O_5S$: C, 65.55; H, 6.42; N, 7.64 and found C, 65.51; H, 6.39; N, 7.26. **FT-IR (ATR), υ** cm^{-1}: 2961 (C-H stretch), 1685 (C=O stretch), 1540, 1490 (C=C). **Mass (m/z):** Calculated: 549.68; Obtained (M+H): 550.25.

*Synthesis of 7-(2,2-dicyanovinyl)-10-(2-ethylhexyl)-10H-phenoxazine-3-carboxylic acid (**PO_3**)*

The starting material 10-(2-ethylhexyl)-7-formyl-10*H*-phenoxazine-3-carboxylic acid (**6**, 0.2 g, 0.54 mmol) was dissolved in 5 mL of DMF and stirred at room temperature for 0.5 h. Then, malononitrile (0.16 mL, 2.72 mmol, 5 eq.) was added to it slowly with constant stirring. Further, the reaction mass was stirred at 90 ^{o}C for 12 h. After completion of the reaction, the solvent was removed under vacuum and the crude product was directly purified using column chromatography technique on 200-400 mess silica using 2:1 hexane/ethyl acetate mixture to get an orange color fine powder as product, yield 78 %, melting point: 260-262 ^{o}C.

^{1}H NMR (400 MHz, DMSO-d6, δ ppm): 12.63 (s, 1H), 8.11 (s, 1H), 7.45-7.40 (m, 1H), 7.25 (s, 1H), 7.13 (s, 1H), 6.94-6.92 (m, 1H), 6.77-6.63 (m, 2H), 3.66-3.53 (d, 2H), 1.34-1.32 (m, 1H), 1.30-1.23 (m, 8H), 0.88-0.81 (t, 6H). **^{13}C NMR** (400 MHz, DMSO-d6, δ ppm): 166.84, 166.50, 162.77, 158.80, 144.43, 144.22, 144.12, 144.02, 139.29, 138.46, 137.08, 135.59, 131.27, 126.70, 126.16, 122.88, 115.80, 114.27, 113.28, 112.32, 75.59, 62.51, 47.05, 36.39, 36.27, 30.24, 30.08, 29.47, 28.49, 28.39, 23.77, 23.65, 22.97, 14.26, 11.18, 11.15. Anal. Calcd. for $C_{25}H_{25}N_3O_3$: C, 72.27; H, 6.06; N, 10.11 and found C, 72.09; H, 6.01; N, 10.06. **FT-IR (ATR), υ** cm^{-1}: 2959, 2926 (C-H stretch), 2222 (C≡N stretch), 1680 (C=O stretch), 1570, 1499 (C=C), 1156 (C-N stretch). **Mass (m/z):** Calculated: 415.48; Obtained (M-H): 414.20.

*Synthesis of (Z)-7-((3-ethyl-4-oxo-2-thioxothiazolidin-5-ylidene)methyl)-10-(2-ethylhexyl)-10H-phenoxazine-3-carboxylic acid (**PO_4**)*

A mixture of 10-(2-ethylhexyl)-7-formyl-10*H*-phenoxazine-3-carboxylic acid (**6**, 0.3 g, 0.81 mmol) *3*-ethylrhodanine (0.15 g, 0.97 mmol), and NH_4OAc (0.69 g, 8.98 mmol) was taken in a dry RB flask and dissolved in 10 mL of glacial acetic acid and further stirred at 110 ^{o}C for 12 h under an argon atmosphere. The reaction completion was monitored by the TLC method. After completion of the reaction, the content was cooled to room temperature and then it was poured into 100 g of crushed ice. The obtained red solid was filtered and dried. The product was purified by column chromatography using silica gel (200-400 mesh) and $CHCl_3$:CH_3OH (10:1) as the mobile phase to get a red color fine powder as product, yield 84 %, melting point: 230-232 ^{o}C.

^{1}H NMR (400 MHz, DMSO-d6, δ ppm): 12.57 (s, 1H), 7.55 (s, 1H), 7.44-7.42 (m, 1H), 7.11-7.04 (m, 2H), 6.89-6.71 (m, 3H), 4.05-4.03 (d, 2H), 3.59-3.33 (m, 2H), 1.31 (m, 1H), 1.22-0.16 (m, 11H), 0.89-0.81 (t, 6H). **^{13}C NMR** (400 MHz, DMSO-d6, δ ppm): 192.75, 192.40, 167.09, 166.68, 166.60, 158.78, 144.65, 144.31, 144.14, 143.91, 140.47, 137.14, 136.41, 135.73, 135.50, 132.51, 126.88, 126.70, 126.57, 124.69, 124.35, 119.84, 119.25, 117.26, 116.77, 116.01, 114.13, 113.22, 47.30, 35.44, 30.20, 28.45, 23.75, 22.98, 14.26, 12.38, 11.20. Anal. Calcd. for $C_{27}H_{30}N_2O_4S_2$: C, 63.50; H, 5.92; N, 5.49 and found C, 63.48; H, 5.91; N, 5.48. **FT-IR (ATR), υ** cm^{-1}: 2960 (C-H stretch), 1682 (C=O stretch), 1582, 1501 (C=C). **Mass (m/z):** Calculated: 510.67; Obtained (M-H): 509.20

*Synthesis of (E)-7-(2-(3-(dicyanomethylene)-5,5-dimethylcyclohex-1-en-1-yl)vinyl)-10-(2-ethylhexyl)-10H-phenoxazine-3-carboxylic acid (**PO$_5$**)*

A mixture of 10-(2-ethylhexyl)-7-formyl-10*H*-phenoxazine-3-carboxylic acid (**6**, 0.2 g, 0.54 mmol), (3,5,5-trimethylcyclohex-2-enylidene) malononitrile (0.4 g, 2.17 mmol), and piperidine (0.5 mL) was taken in a dry RB flask and dissolved in 10 mL of acetonitrile and further stirred at 80-85 ^{o}C for 12 h under an argon atmosphere. The reaction completion was monitored by the TLC method. After completion of the reaction, the content was cooled to room temperature, and then it was poured into 100 g of crushed ice. Further, the product was extracted with ethyl acetate (3 × 30 mL). The crude product was purified by column chromatography using silica gel (200-400 mesh) and $CHCl_3$:CH_3OH (10:1) as the mobile phase to get pink color fine powder as product, yield 81 %, melting point: 280-282 ^{o}C.

^{1}H NMR (400 MHz, DMSO-d6, δ ppm): 12.74 (s, 1H), 7.40-7.38 (m, 1H), 7.28 (s, 1H), 7.24 (s, 1H), 7.13 (s, 2H), 7.08 (s, 1H), 6.83 (s, 1H), 6.80-6.76 (m, 2H), 4.90-3.88 (d, 2H), 1.52 (s, 4H), 1.40-1.16 (m, 8H), 1.01 (s, 6H), 0.89-0.80 (t, 6H). **^{13}C NMR** (400 MHz, DMSO-d6, δ ppm): 164.47, 162.88, 162.74, 156.69, 150.76, 145.08, 144.47, 144.44, 134.76, 134.21, 125.85, 129.53, 128.71, 127.81, 125.20, 125.05, 124.20, 123.04, 122.95, 122.77, 122.58, 122.51, 120.71, 115.80, 111.34, 110.60, 110.53. Anal. Calcd. for $C_{34}H_{37}N_3O_3$: C, 76.23; H, 6.96; N, 7.84 and found C, 76.18; H, 6.91; N, 7.78. **FT-IR (ATR), υ** cm^{-1}: 3341 (-O-H stretching), 2956, 2868 (C-H stretch), 2216 (C≡N stretch), 1552, 1500 (C=C stretch). **Mass (m/z):** Calculated: 535.68; Obtained (M-H): 534.20.

*Synthesis of (Z)-10-(2-ethylhexyl)-7-((2-oxoindolin-3-ylidene)methyl)-10H-phenoxazine-3-carboxylic acid (**PO$_6$**)*

A mixture of 10-(2-ethylhexyl)-7-formyl-10*H*-phenoxazine-3-carboxylic acid (**6**, 0.3 g, 0.81 mmol), 2-oxindole (0.09 g, 0.81 mmol), and piperidine (0.5 mL) was taken in a dry RB flask and dissolved in 8-10 mL of ethanol and further stirred at 80 ^{o}C for 12 h under an argon atmosphere. After completion of the reaction, the content was cooled to room temperature. The precipitated solid was filtered and washed with pre-cooled ethanol. The obtained dyes were purified by column chromatography with a 2:1 hexane:ethyl acetate solvent system to get yellowish color fine powder as product, yield 76 %, melting point: 266-268 ^{o}C.

^{1}H NMR (400 MHz, DMSO-d6, δ ppm): 12.60 (s, 1H), 8.11 (s, 1H), 7.47-7.45 (m, 2H), 7.26-7.25 (m, 1H), 7.13-7.12 (m, 2H), 7.06-7.05 (m, 2H), 6.79-6.73 (m, 3H), 6.63 (m, 1H), 3.66-3.64 (d, 1H), 3.55-3.53 (d, 1H), 1.34-1.23 (m, 9H), 0.88-0.81 (t, 6H). **^{13}C NMR** (400 MHz, DMSO-d6, δ ppm): 163.09, 163.00, 161.30, 154.87, 151.41, 144.24, 143.23, 138.44, 136.23, 135.79, 126.46, 126.40, 125.22, 119.82, 116.00, 114.42, 113.79, 47.32, 36.40, 30.16, 29.07, 28.49, 23.73, 22.98, 14.27, 11.20. Anal. Calcd. for $C_{30}H_{30}N_2O_4$: C, 74.67; H, 6.27; N, 5.81 and found C, 74.60; H, 6.18; N, 5.78. **FT-IR (ATR), υ** cm^{-1}: 2959, 2869 (C-H stretch), 1694 (C=O stretch), 1585, 1502 (C=C). **Mass (m/z):** Calculated: 482.57; Obtained (M-H): 481.25.

Device fabrication procedures

Fabrication of p-type DSSCs sensitized with dyes PO$_{1-6}$

The procedure used for the fabrication of NiO-based *p*-type DSSCs is as follows. The FTO coated glass substrates were successively cleaned by sonication in detergent and acidified ethanol for 10 min before annealing at 450 °C for 30 min. A NiO dense layer was prepared by spin-coating onto the clean substrates of a 0.5 M nickel acetate solution containing 0.5 M ethanolamine in methoxyethanol at 3000 rpm for 30 s followed by thermal treatment at 500 °C for 0.5 hr. Then, NiO paste was screen printed on top of FTO substrates containing NiO dense layer (30±5 nm). Here, the NiO screen-printing paste was produced by preparing a slurry of 3 g of NiO nanopowder (Inframat) suspended in 10 mL of freshly distilled ethanol and ball-milled (500 rpm) for 24 h. Further, the slurry was mixed with 10 mL of 10 wt % ethanolic ethyl cellulose (Sigma Aldrich) solution and 20 mL terpineol. The solvent was removed using a rotary evaporator. The NiO films were annealed at 450°C for 30 min and thickness was found to be 3.5 µm±50 nm. In continuation, the NiO electrodes were soaked in a solution of nickel acetate in ethanol (20 mM) with 1% ethanolamine for 30 min at

60 °C followed by ethanol rinsing and drying in air. The electrodes NiO were finally annealed at 120 °C for 60 min, then were dipped in a solution of the dye (0.3 mmol L^{-1} in CH_3CN) and stored at room temperature overnight.

Platinum counter electrodes were prepared by depositing a few drops of an isopropanol solution of hexachloroplatinic acid in distilled isopropanol (2 mg per mL) on FTO plates (TEC7, Solaronix). Substrates were then fired at 375 °C for 30 min. The photocathode and the counter electrode were placed on top of each other and sealed using a thin transparent film of Surlyn polymer (DuPont, 25 µm) as a spacer. A drop of the electrolyte was introduced through a predrilled hole in the counter electrode by vacuum backfilling; the hole was then sealed by a glass stopper with Surlyn. The cell had an active area of 0.25 cm^2. The electrolyte used is composed of 0.1 M I_2 and 1 M lithium iodide in acetonitrile.

Acknowledgments

The authors are thankful to NITK, Surathkal, India, for providing necessary laboratory facilities. The authors are also indebted to the CCIPL/GLICID computational centre installed in Nantes for the very generous allocation of computational resources. We also thank Conseil Régional des Pays de la Loire for Financial support *via* LUMOMAT Project.

Declaration of Competing Interest

The authors declare that they have no known competing financial interests or personal relationships that could have appeared to influence the work reported in this paper.

Reference

[1] B. O'Regan and M. Gratzel, *Nature* **1991**, *353*, 737-740.
[2] A. Hagfeldt, G. Boschloo, L. Sun, L. Kloo, H. Pettersson, *Chem. Rev.* **2010**, *110*, 6595–6663.
[3] F. Gao, C. L. Yang, M. S. Wang, X. G. Ma, W. W. Liu, *Spectrochim. Acta A Mol. Biomol. Spectrosc.* **2019**, *206*, 216–223.
[4] P. Ferdowsi, Y. Saygili, F. Jazaeri, T. Edvinsson, J. Mokhtari, S. M. Zakeeruddin, Y. Liu, M. Grätzel, A. Hagfeldt, *ChemSusChem* **2020**, *13*, 212–220.
[5] E. Ferreira, P. L. Poul, N. Cabon, B. Caro, F. R.-L. Guen, Y. Pellegrin, A. Planchat, F. Odobel, *Tetrahedron Lett.* **2017**, *58*, 995–999.

[6] J. He, H. Lindström, A. Hagfeldt and S.-E. Lindquist, *J. Phy. Chem. B*, **1999**, *103*, 8940-8943.
[7] F. Odobel, L. L. Pleux, Y. Pellegrin, E. Blart, *Acc. Chem. Res.* **2010**, *43*, 1063–1071.
[8] J.-F. Lefebvre, X.-Z. Sun, J. A. Calladine, M. W. George, E. A. Gibson, *Chem. Commun.* **2014**, *50*, 5258-5260.
[9] F. Wu, L. Zhu, S. Zhao, Q. Song, C. Yang, *Dyes Pigm.* **2016**, *124*, 93–100.
[10] L. L. Pleux, A. L. Smeigh, E. Gibson, Y. Pellegrin, E. Blart, G. Boschloo, A. Hagfeldt, L. Hammarström, F. Odobel, *Energy Environ. Sci.* **2011**, *4*, 2075–2084.
[11] Y. Farré, F. Maschietto, J. Föhlinger, M. Wykes, A. Planchat, Y. Pellegrin, E. Blart, I. Ciofini, L. Hammarström, F. Odobel, *ChemSusChem* **2020**, *13*, 1844–1855.
[12] Y. Farré, L. Zhang, Y. Pellegrin, A. Planchat, E. Blart, M. Boujtita, L. Hammarström, D. Jacquemin, F. Odobel, *J. Phys. Chem. C* **2016**, *120*, 7923–7940.
[13] F. Sahiner, A. K. Ali, S. Denizalti, Z. Kandemir, S. Erten-Ela, *New J. Chem.* **2020**, *44*, 15526–15537.
[14] L. Zhu, H. B. Yang, C. Zhong, C. M. Li, *Dyes Pigm.* **2014**, *105*, 97–104.
[15] Y. Farré, M. Raissi, A. Fihey, Y. Pellegrin, E. Blart, D. Jacquemin, F. Odobel, *ChemSusChem* **2017**, *10*, 2618–2625.
[16] L. Q. Bao, H. Phuong, C. T. T. Thuy, J. W. Lee, J. H. Kim, S. Thogiti, *Mol. Cryst. Liq.* **2017**, *653*, 109–117.
[17] Y. Farré, M. Raissi, A. Fihey, Y. Pellegrin, E. Blart, D. Jacquemin, F. Odobel, *Dyes Pigm.* **2018**, *148*, 154–166.
[18] D. Xiong, W. Zhang, X. Zeng, Z. Xu, W. Chen, J. Cui, M. Wang, L. Sun, Y. B. Cheng, *ChemSusChem* **2013**, *6*, 1432–1437.
[19] F. Odobel, Y. Pellegrin, *J. Phys. Chem. Lett.* **2013**, *4*, 2551–2564.
[20] B. Xu, S. Wrede, A. Curtze, L. Tian, P. B. Pati, L. Kloo, Y. Wu, H. Tian, *ChemSusChem* **2019**, *12*, 3243–3248.
[21] J. Warnan, Y. Pellegrin, E. Blart, L. Zhang, A. Brown, L. Hammarström, D. Jacquemin, F. Odobel, *Dyes Pigm.* **2014**, *105*, 174–179.
[22] T. T. T. Pham, S. K. Saha, D. Provost, Y. Farré, M. Raissi, Y. Pellegrin, E. Blart, S. Vedraine, B. Ratier, D. Aldakov, F. Odobel, J. Bouclé, *J. Phys. Chem. C* **2017**, *121*, 129–139.
[23] Y. Pellegrin, L. L. Pleux, E. Blart, A. Renaud, B. Chavillon, N. Szuwarski, M. Boujtita, L. Cario, S. Jobic, D. Jacquemin, F. Odobel, *J. Photochem. Photobiol. A: Chem.* **2011**, *219*, 235–242.
[24] H. Tian, I. Bora, X. Jiang, E. Gabrielsson, K. M. Karlsson, A. Hagfeldt, L. Sun, *J. Mater. Chem. A* **2011**, *21*, 12462–12472.
[25] H. Tian, X. Yang, J. Cong, R. Chen, J. Liu, Y. Hao, A. Hagfeldt, L. Sun, *Chem. Comm.* **2009**, 6288–6290.
[26] K. M. Karlsson, X. Jiang, S. K. Eriksson, E. Gabrielsson, H. Rensmo, A. Hagfeldt, L. Sun, *Chem. Eur. J.* **2011**, *17*, 6415–6424.
[27] H. Tan, C. Pan, G. Wang, Y. Wu, Y. Zhang, Y. Zou, G. Yu, M. Zhang, *Org. Electron.* **2013**, *14*, 2795–2801.
[28] Y. Hao, H. Tian, J. Cong, W. Yang, I. Bora, L. Sun, G. Boschloo, A. Hagfeldt, *ChemPhysChem* **2014**, *15*, 3476–3483.
[29] S. Ramkumar, S. Anandan, *RSC Adv.* **2013**, *3*, 21535–21543.
[30] R. M. Pearson, C. H. Lim, B. G. McCarthy, C. B. Musgrave, G. M. Miyake, *J. Am. Chem. Soc.* **2016**, *138*, 11399–11407.
[31] A. Morandeira, J. Fortage, T. Edvinsson, L. L. Pleux, E. Blart, G. Boschloo, A. Hagfeldt, L. Hammarström, F. Odobel, *J. Phys. Chem. C* **2008**, *112*, 1721–1728.

[32] S. I. V. Dijk, C. P. Groen, F. Hartl, A. M. Brouwer, J. W. Verhoeven, *J. Am. Chem. Soc.* **1996**, *118*, 35, 8425–8432.
[33] S. M. Dyar, E. A. Margulies, N. E. Horwitz, K. E. Brown, M. D. Krzyaniak, M. R. Wasielewski, *J. Phys. Chem. B* **2015**, *119*, 13560–13569.
[34] M. Gennari, F. Légalité, L. Zhang, Y. Pellegrin, E. Blart, J. Fortage, A. M. Brown, A. Deronzier, M. N. Collomb, M. Boujtita, D. Jacquemin, L. Hammarström, F. Odobel, *J. Phys. Chem. Lett.* **2014**, *5*, 2254–2258.
[35] J. V. Vaghasiya, K. K. Sonigara, J. Prasad, T. Beuvier, A. Gibaud, S. S. Soni, *J. Mater. Chem. A* **2017**, *5*, 5373–5382.
[36] G. Wang, Y. Hu, Y. Chen, X. Liao, Z. Li, X. Chen, X. Wang, B. Liu, *ACS Omega* **2020**, *5*, 22621–22630.
[37] K. S. Keremane, A. V. Adhikari, *Electrochemical Science Advances* **2021**, *1*, DOI 10.1002/elsa.202000036.
[38] K. S. Keremane, R. Rao, A. V. Adhikari, *Photochem. Photobiol.* **2021**, *97*, 289–300.
[39] K. S. Keremane, P. Naik, A. V. Adhikari, *J. Nano- Electron. Phys.* **2020**, *12*, DOI 10.21272/JNEP.12(2).02039.
[40] Z. D. Sun, J. S. Zhao, K. Ayyanar, X. H. Ju, Q. Y. Xia, *RSC Adv.* **2020**, *10*, 10569–10576.
[41] K. S. Keremane, I. M. Abdellah, P. Naik, A. El-Shafei, A. V. Adhikari, *Phys. Chem. Chem. Phys.* **2020**, *22*, 23169–23184.
[42] P. Naik, A. Planchat, Y. Pellegrin, F. Odobel, A. V. Adhikari, *Sol. Energy* **2017**, *157*, 1064–1073.
[43] L. Nhon, A. D. Taggart, T. Moot, M. K. Brennaman, P. Jagadesan, K. S. Schanze, J. F. Cahoon, J. R. Reynolds, *Chem. Mater.* **2020**, *32*, 8158–8168.
[44] K. Hu, R. N. Sampaio, J. Schneider, L. Troian-Gautier, G. J. Meyer, *J. Am. Chem. Soc.* **2020**, *142*, 16099–16116.
[45] F. Odobel, L. L. Pleux, Y. Pellegrin, E. Blart, *Acc. Chem. Res.* **2010**, *43*, 1063–1071.
[46] D. Ameline, S. Diring, Y. Farre, Y. Pellegrin, G. Naponiello, E. Blart, B. Charrier, D. Dini, D. Jacquemin, F. Odobel, *RSC Adv.* **2015**, *5*, 85530-85539.
[47] M. J. Frisch, *et al*. Gaussiañ16 Rev. A.03, **2016**. Gaussian Inc. Wallingford CT.
[48] C. Adamo, V. Barone, *J. Chem. Phys.*, **1999**, *110*, 6158–6170.
[49] J. Tomasi, B. Mennucci, R. Cammi, *Chem. Rev.*, **2005**, *105*, 2999–3093.
[50] T. Yanai, D. P. Tew, N. C. Handy, *Chem. Phys. Lett.*, **2004**, *393*, 51–57.
[51] C. A. Guido, A. Chrayteh, G. Sclamani, B. Mennucci, D. Jacquemin *J. Chem. Theory Comput.* **2021**, *17*, 5155−5164.
[52] T. Le Bahers, C. Adamo, I. Ciofini, *J. Chem. Theory Comput.* **2011**, *7*, 2498−2506.